Ti:Sapphire Lasers

Albert Liu
University of Michigan, Ann Arbor

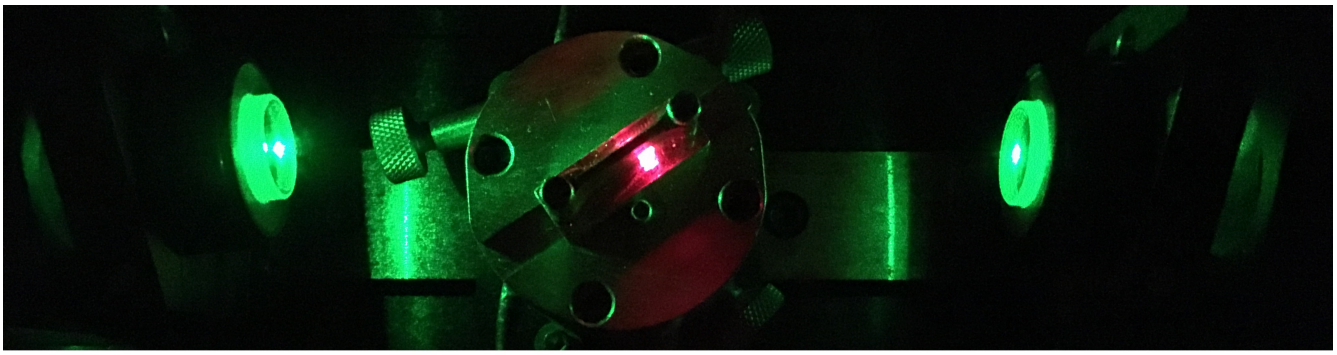

Figure 1. The cavity of a Ti:Sapph laser built by the author. Shown are the curved mirrors and the Ti:Sapph laser crystal oriented at the Brewster angle.

Contents

Introduction

In the last few decades, the attention of the science community has shifted increasingly towards understanding the fastest processes in nature. Chemical bond formation/breaking, carrier dynamics, and other (sub)picosecond processes have found increasing applications in fields such as material science, diffraction-limited imaging, and quantum device physics, just to name a few. To study these ultra-fast processes one needs a probe of simliar or shorter time-scale. The natural method is to use the fastest process in nature - light. Ultrafast pulses of light can now be generated by lasers, and the clear workhorse that has emerged is the Ti:Sapphire laser.

1. Basic Properties of Ti:Sapphire

We begin by examining the crystal structure of Ti:Sapphire. Pure sapphire (Al_2O_3) exists as a trigonal crystal, and Titanium dopants (typically at a density $\approx 10^{25} m^{-3}$) replace Aluminum atoms at their lattice sites:

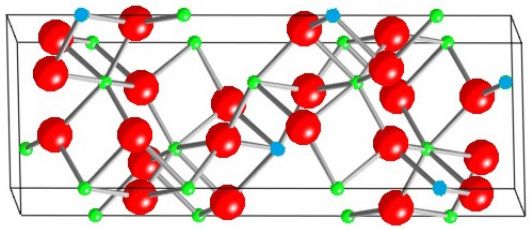

Figure 2. The atomic structure of Ti:Sapphire. The red, green, and blue atoms are Oxygen, Aluminum, and Titanium atoms respectively.

Each Titanium atom bonds to six neighboring Oxygen atoms, so the Titanium atoms themselves exist effectively as Ti^{3+} ions. The electronic structure is thus an inert argon shell with a single $3d$-orbital electron. In total there are five $3d$-orbital arrangements, and they are then split into two upper and lower energy manifolds via Stark shift due to the fields of surrounding Oxygen atoms and spin-orbit coupling:

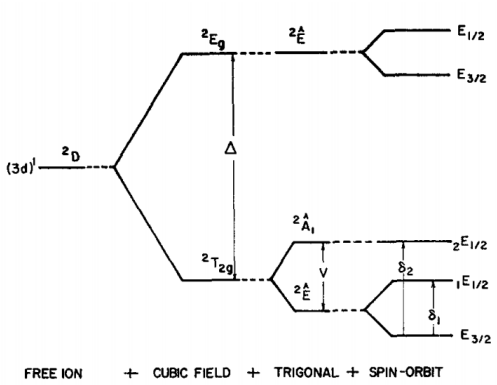

Figure 3. Energy splitting of free Ti^{3+} ion levels. From [1].

We see that the cubic field from the surrounding Oxygen atoms splits the 5 free levels into an excited doublet level and ground state triplet level, denoted as E and T respectively . The further fine splitting via the trigonal field and spin-orbit coupling we can neglect. We can gain further insight by plotting the energies of E and T as a function of the Ti^{3+} ion's displacement from its equilibrium lattice position:

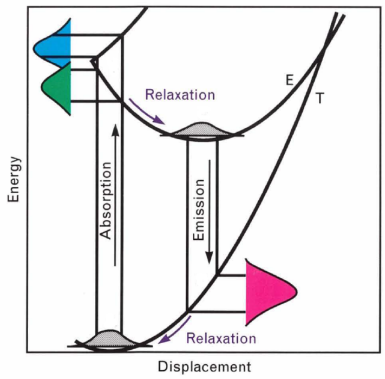

Figure 4. The displacement domain bandstructure of the upper doublet and lower triplet levels of Ti:Sapphire. From [2].

As a result of the Jahn-Teller effect, the energies are distorted in the displacement domain. The continuum of energies formed by the upper and lower levels are sometimes called **vibronic levels**[1], since the electron can relax between them via emission of phonons and displacement of the whole Ti^{3+} ion. At equilibrium, the $3d$ electron in the ground state T can be excited into an upper vibronic metastable continuum in E by absorption in the green/blue. The electron will then decay between the vibronic levels very quickly into the upper lasing level. The distorted bandgap is now smaller, allowing for emission in the red. Another phonon emission process then allows for the Ti^{3+} to return to its equilibrium position. We can therefore approximate the entire system as an effective four-level system, with the lasing and metastable levels corresponding to different lattice configurations of the Ti^{3+} ion[2]. Labeling the ground and upper metastable states as energy levels E_1 and E_4 respectively, and the lower and upper lasing levels as E_2 and E_3 respectively, the lifetimes of each level are given by[3]:

$$\tau_4 \approx \tau_{43} \approx 0.1ps \qquad \tau_3 \approx \tau_{32} \approx 3.2\mu s \qquad \tau_{21} \approx 0.1ps \tag{1}$$

where we have made the approximation that no $E_4 \to E_2$, $E_4 \to E_1$, or $E_3 \to E_1$ transitions occur, since these can only happen via phonon-assisted emission.

[1] This is why Ti:Sapphire lasers fall into a subclass of lasers known as **vibronic lasers**.

2. Pumping Analysis

This section will heavily use results derived in [3]. By standard four-level rate equation analysis, we find the populations of the upper and lower lasing levels N_3 and N_2 to be related by:

$$N_2 = \beta N_3 \quad \text{where} \quad \beta \approx \frac{\tau_{21}}{\tau_{32}} = 3.125x10^{-8} \tag{2}$$

We then note that the fluorescence quantum efficiency is approximately unity[4]:

$$\eta = \frac{\tau_4 \tau_3}{\tau_{43}\tau_{rad}} \approx 1 \tag{3}$$

The four level system steady-state population inversion is derived in Appendix A. In the limit $\beta \approx 0$ and $\eta \approx 1$, and ground/excited state degeneracies $g_1 = 3$ and $g_4 = 2$, we find:

$$\begin{aligned}
\frac{N_3 - N_2}{N} &= \frac{W_{14}\tau_4\gamma_{43}}{\left(2+\frac{g_1}{g_4}\right)W_{14}\frac{\tau_4}{\tau_3} + \frac{1}{\tau_3} + W_{14}\tau_4\gamma_{43}(1+\beta)} - \frac{g_3}{g_2}\frac{W_{14}\tau_4\gamma_{43}}{\left(2+\frac{g_1}{g_4}\right)W_{14}\frac{\tau_4}{\tau_3\beta} + \frac{1}{\tau_3\beta} + W_{14}\tau_4\gamma_{43}\left(1+\frac{1}{\beta}\right)} \\
&\approx \frac{W_{14}\tau_4\gamma_{43}}{\left(2+\frac{g_1}{g_4}\right)W_{14}\frac{\tau_4}{\tau_3} + \frac{1}{\tau_3} + W_{14}\tau_4\gamma_{43}} \\
&= \frac{W_{14}}{W_{14}\left(\frac{7}{2}\frac{\tau_{43}}{\tau_{32}}+1\right) + \frac{1}{\tau_3}}
\end{aligned} \tag{4}$$

Recalling the following formula for the pump rate:

$$W_{14} = W_p = \frac{\sigma I_{pump}}{\hbar\omega} \tag{5}$$

We can rewrite the population inversion in terms of the stimulated emission cross-section:

$$\frac{N_3 - N_2}{N} = \frac{\sigma I_{pump}}{\sigma I_{pump}\left(\frac{7}{2}\frac{\tau_{43}}{\tau_{32}}+1\right) + \frac{\hbar\omega}{\tau_3}} \tag{6}$$

The cross-section for Ti:Sapphire is approximately $\sigma = 3x10^{-19}cm^2$, and assuming a pump at $\lambda = 532nm$ focused to a spot size of $200\mu m^2$ on the crystal, we plot the normalized steady-state population inversion below:

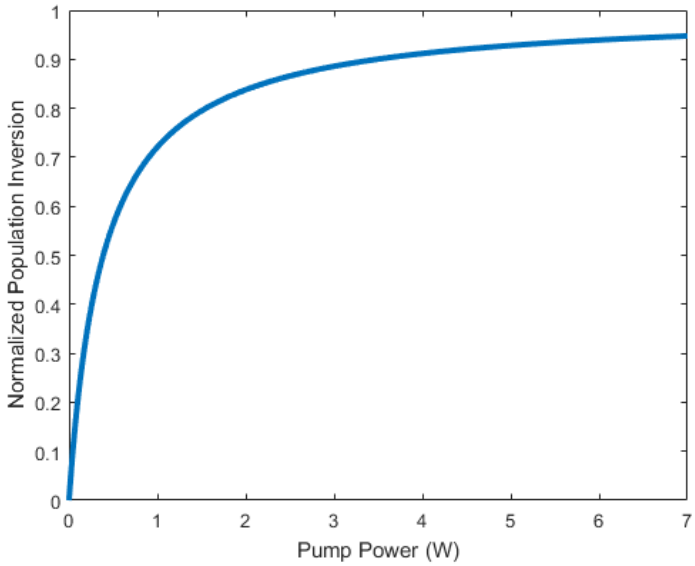

Figure 5. Normalized population inversion plotted as a function of pump power.

where we have taken into account the reflection loss of $\approx 1\%$ with the crystal oriented at the Brewster angle. The pump power along the x-axis refers to the input pump power, before any reflection losses.

3. Laser Cavity

To design our Ti:Sapphire laser, we use a folded geometry as shown:

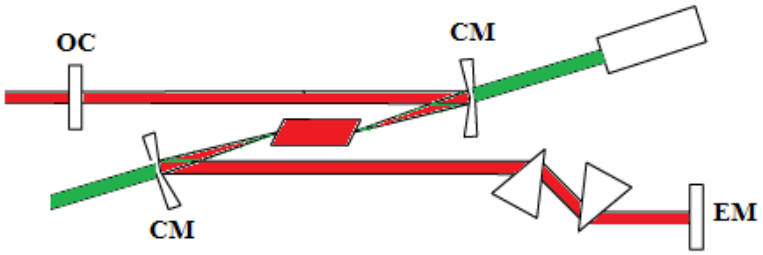

Figure 6. Folded geometry laser cavity. The cavity consists of two curved mirrors (CM), one end mirror (EM), one output coupler (OC), and two prisms for dispersion compensation. There is also an additional lens of focal length $f = 13cm$ before the first curved mirror that focuses the pump beam into the crystal.

Where the curved mirrors have a radius of curvature $R = 10cm$ and the end mirrror and output coupler are plane mirrors. For curved mirrors and an end mirror of reflectivities $R = 99\%$, and an output coupler of reflectivity $R = 93\%$, we define in delta notation:

$$\delta_{CM} = \delta_{EM} = ln\left(\frac{1}{.99}\right) = .0101 \qquad \delta_{OC} = ln\left(\frac{1}{.93}\right) = .073 \tag{7}$$

where we used the reflectivities around the operating wavelength of $\lambda = 800nm$. Assuming negligible intracavity loss, we find a total cavity loss factor:

$$\delta_c = 2\delta_{CM} + \delta_{CM} + \delta_{OC} = .1033 \tag{8}$$

We can now find the pump threshold power:

$$P_{th} = \frac{V}{\eta_p}\frac{N_{3,th}}{\Delta N_{th}}\frac{\omega_p}{\omega_a}\frac{\gamma_3}{\gamma_{rad}}\frac{4\pi^2}{3^*}\frac{\hbar\Delta\omega_a}{\lambda^3}\frac{c\delta_c}{p_m} \approx 131.45mW \tag{9}$$

where we've used the values:

- $\eta_p \approx .9$ (see reference pg. 580 of [5])
- $N_{3,th} \approx \Delta N_{th}$ (lower lasing level empties quickly)
- $\Delta\omega_a = \gamma_3 + \frac{2}{T_2} \approx \frac{2}{T_2}$ where $T_2 \approx 7.4fs$ (dephasing dominates linewidth, see reference [6])
- $\gamma_3 \approx \gamma_{rad}$ (transition from upper lasing level to ground state requires simultaneous phonon/photon emission).
- $p_m \approx 2.15mm$ (actual crystal length of the author's laser)
- $3^* = 1$ (atoms randomly aligned)
- $V = p_m(200\mu m^2) = 4.3x10^{-13}m^3$ (assuming a spot size of $200\mu m^2$)

This pump power is much smaller than typical threshold powers reported[7], which are usually around 1W. This discrepancy may be due to a variety of factors, such as pump power loss due to imperfect Brewster scattering (requiring a higher pump power), a lower quantum efficiency than used due to increased operating temperature ([8] cites quantum efficiencies as low as $\eta_p \approx .68$ at $T = 325K$), non-negligible intra-cavity losses (due to material losses in the prism compressor, scattering losses, etc.), and imperfect mode overlap between the pump and signal beams (due to differences in refractive index).

4. CW Operation

We now cite a typical value for the cross-section of Ti:Sapphire at its operating wavelength[9]:

$$\sigma \approx 3x10^{-23} m^2 \tag{10}$$

which gives a gain saturation intensity:

$$I_{sat} = \frac{\hbar\omega_a}{\sigma\tau_{eff}} = 2.58x10^9 \frac{W}{m^2} = 25.8\frac{kW}{cm^2} \tag{11}$$

The typically density of Titanium dopants[10] is $N \approx 10^{25} m^{-3}$, which we approximate as the ground state population $(N_1 \approx N)$. We now define a few quantities:

$$R_p \approx \eta_p W_p N = \eta_p \frac{\sigma}{\hbar\omega_a} N I_{pump} = (6.82x10^{20}) I_{pump} \tag{12}$$

$$\Delta N_0 \approx R_p \tau_3 = 2.18x10^{15} I_{pump} \tag{13}$$

$$\alpha_{m0} = \frac{\Delta N_0 \sigma}{2} = (3.28x10^{-8}) I_{pump} \tag{14}$$

Since all of our mirrors are well above 90% reflectivity, we can derive the circulating intensity in the small output coupling approximation. In this approximation, the circulating intensity is given by:

$$\begin{aligned} I_{circ} &= \left[\frac{2\alpha_{m0} p_m}{\delta_c} - 1\right] \frac{I_{sat}}{2} \\ &= \left[(1.37x10^{-9}) I_{pump} - 1\right] (1.26x10^9) \end{aligned} \tag{15}$$

and the power coupled through the 7% transmission output coupler is simply:

$$I_{out} = 0.07 I_{circ} \tag{16}$$

Assuming that the signal beam has the same spot size of the pump beam $(200\mu m^2)$ inside the crystal, which usually will not be the case, we find:

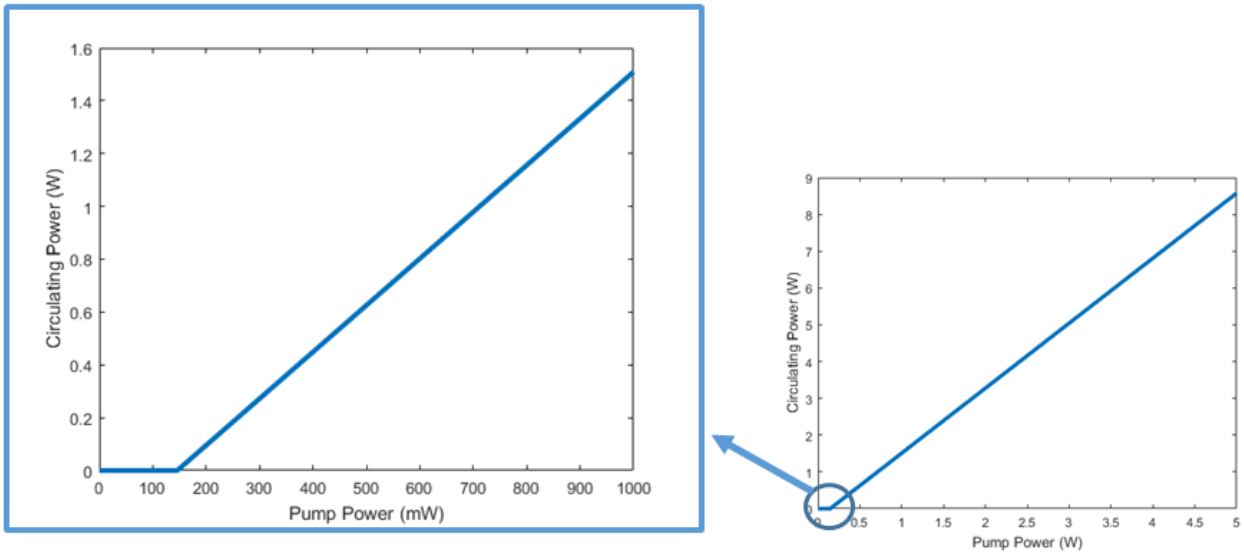

Figure 7. Circulating power inside cavity.

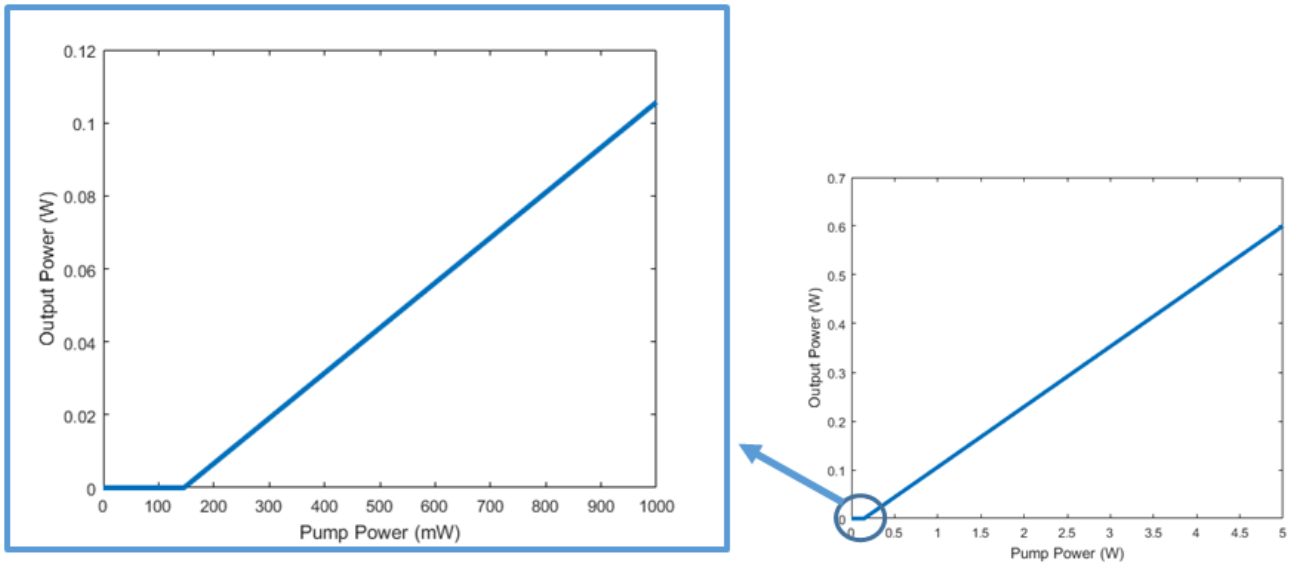

Figure 8. Output power inside cavity.

From the plots, we can immediately see that the threshold pump power is approximately $P_{th} \approx 140mW$, which agrees quite nicely with the threshold power found earlier.

As a second check, we can also calculate the normalized threshold population inversion:

$$\frac{\Delta N_{th}}{N} = \frac{\delta_c}{\sigma p_m N} \approx .16 \tag{17}$$

The normalized population inversion at low pump power is plotted below (using the same formula derived in the first section):

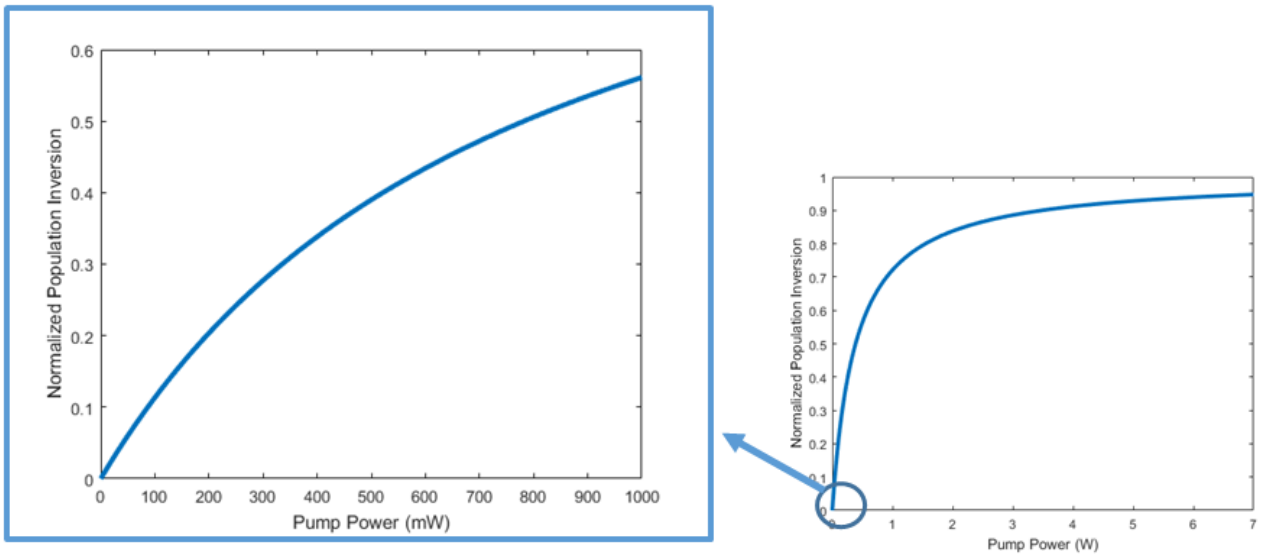

Figure 9. Low pump power population inversion.

We see that the normalized population inversion reaches $\frac{\Delta N}{N} \approx .16$ at a pump power of approximately $150mW$. This is a bit higher than the previous threshold values found, but still agrees nicely with the derived numbers.

5. Pulsed Operation

The main reason why Ti:Sapphire lasers have become so ubiquitous in the laser community is its excellent mode-locking characteristics that allow it to generate femto-second pulses with great ease and stability. Although in principle one should mode-match the transverse pump and signal transverse beam profiles while compensating the cavity dispersion, in practice experimental error makes it more practical to optimize the cavity mirror positions by trial and error. However, there are two parameters that should be calculated before hand - the curved mirror tilt for astigmatism compensation and the prism compressor separation for dispersion compensation.

Astigmatism Compensation

The astigmatism in the cavity is due to the longitudinal and sagittal ray bundles of the signal beam experiencing different angles of incidences at the Ti:Sapphire crystal. Because the crystal is cut at the Brewster angle, the longitudinal ray bundles will "see" an angle of incidence greater than the angle that the sagittal ray bundles see. To compensate for the astigmatic distortion of the beam, one therefore needs to tilt the curved mirrors so that the different ray bundles are focused by different radii of curvature and the distortion is compensated. To determine the tilt, we cite an equation[2] from [11]:

$$\frac{(n^2-1)\sqrt{n^2+1}p_m}{Rn^4} = sin(\theta)tan(\theta) \tag{18}$$

where the angle is defined in figure 11:

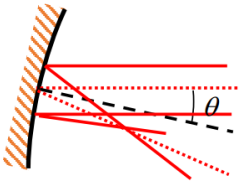

Figure 10. Definition of the angle θ.

For $R = 10cm$, $p_m = 2.15mm$, and $n = 1.76$, we can solve for θ numerically by plotting both sides of equation (20):

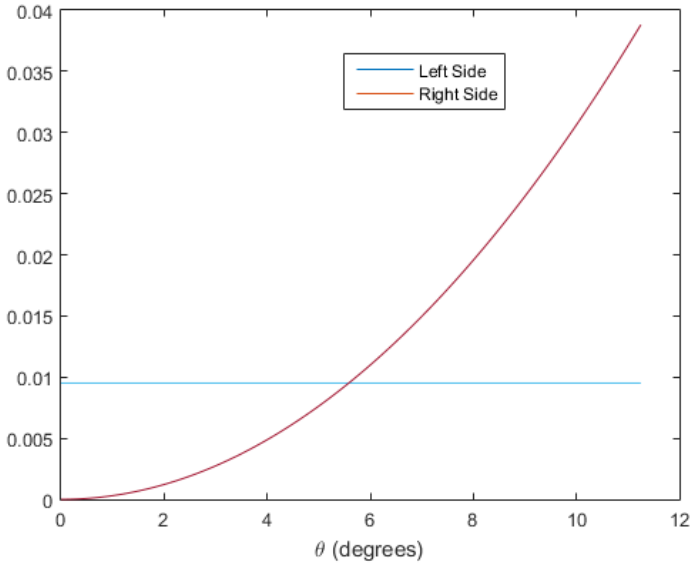

Figure 11. Left and right sides of equation (20) as a function of θ.

We see that to compensate for the astigmatism, we need to tilt each mirror at angle $\theta \approx 5.8^\circ$ according to figure 11. Though astigmatism compensation should be considered for optimal CW operation, it is critical for pulsed operation since the pulse energy will be throttled and mode-locking will become much more difficult.

[2] You may notice that there is a factor of 2 missing from the left side in comparison to the original equation in [11]. This is because they consider only one tilted mirror, while our setup involves two mirrors tilted symmetrically.

Dispersion Compensation

The final consideration is pulse separation in the compressor. The compressor is necessary for pulsed operation, since intracavity dispersion arising from mainly the Ti:Sapphire crystal and cavity mirrors will result in pulse broadening. To compensate this dispersion, we use a prism pair to add dispersion of the opposite sign into the cavity - the prism separation and thickness through which the beam travels will determine the amount of dispersion the prism pair provides.

To compensate the intracavity dispersion, we first must calculate the amount of dispersion inside the prism-less cavity. Assuming that we use metallic mirrors which contribute negligible dispersion, the only significant dispersion source will be the Ti:Sapphire crystal. The Sellmeier equation for Ti:Sapphire is given by:

$$n^2 = 1 + \frac{1.431\lambda^2}{\lambda^2 - .073^2} + \frac{0.651\lambda^2}{\lambda^2 - 0.119^2} + \frac{5.341\lambda^2}{\lambda^2 - 18.028^2} \tag{19}$$

We can also calculate the derivatives at the operating wavelength:

$$n(\lambda_0) = 1.76 \qquad \left.\frac{dn}{d\lambda}\right|_{\lambda=.8\mu m} = -0.0627 \qquad \left.\frac{d^2n}{d\lambda^2}\right|_{\lambda=.8\mu m} = 0.032 \qquad \left.\frac{d^3n}{d\lambda^3}\right|_{\lambda=.8\mu m} = -0.0628$$

In typical experiments, compensation of dispersion up to the second and third orders is sufficient. These are given by:

$$\begin{aligned}\phi'' &= \frac{d^2\beta}{d\omega^2} p_m \\ &= \frac{\lambda^3}{2\pi c^2}\frac{d^2n}{d\lambda^2} p_m = 63.17 fs^2\end{aligned} \tag{20}$$

$$\begin{aligned}\phi^{(3)} &= \frac{d^3\beta}{d\omega^3} p_m \\ &= -\frac{\lambda^2}{4\pi^2 c^3}\left(3\lambda^2\frac{d^2n}{d\lambda^2} + \lambda^3\frac{d^3n}{d\lambda^3}\right) p_m = -38.31 fs^3\end{aligned} \tag{21}$$

For the prism material, we will use fused silica. The second and third order dispersion as a function of prism separation L and the thickness through which the beam travels d (both in cm) is given by[12]:

$$\phi'' = 683.56d - 10.81L \tag{22}$$

$$\phi^{(3)} = 522.88d - 12.14L \tag{23}$$

To compensate the cavity dispersion, we set equation (20) equal to the negative value of equation (22), and we also do the same with equation (21) and (23). This gives a system of two equations to solve simultaneously, which gives:

$$d = .538cm \quad \text{and} \quad L = 39.92cm \tag{24}$$

Cavity Alignment for Mode-locking

Once the prisms and mirror tilt are aligned in the cavity, there is one final step to mode-lock the laser. Assuming that the cavity is optimized for CW operation, the next step is to begin moving the second curved mirror in towards the Ti:Sapphire crystal. The purpose of shifting the curved mirror is to make the cavity unstable for low intensity CW light, while stable for the Kerr focused high intensity pulses. A general procedure is to direct the Ti:Sapphire output onto a fast photodiode (GHz resolution), and observe the signal on an oscilloscope. As one moves the mirror inwards, tapping the end mirror should result in flashes of a pulse train appear on the oscilloscope display. Alternating between moving the mirror and tapping the end mirror should make it obvious which direction one should go in. An alternative to using a photodiode is to use a spectrometer instead, in which tapping the end mirror should briefly broaden the narrow CW spectrum into a broad pulse bandwidth.

6. Outlook

Since its discovery by Moulton in 1986[13], the Ti:Sapphire laser has emerged as the primary workhorse laser in ultrafast science. Current "hot" fields such as frequency comb generation[14] and attosecond science via high harmonic generation[15] rely on Ti:Sapphire as a robust source for ultrafast pulses, and even when not used Ti:Sapphire is used as a standard benchmark. Recent advances in fiber technology, especially the advent of the photonic crystal fiber[16], have sparked much interest in utilizing the broad bandwidth of Ti:Sapphire in supercontinuum generation. Furthermore, the Ti:Sapphire crystal offers a unique blend of desirable physical properties, such as high thermal conductivity for effective heat dissipation, a large nonlinear index (suitable for Kerr lens mode-locking), and it being the third hardest mineral (9/10 on the Mohs scale) which provides remarkable robustness. There is not a single field of ultrafast science that has not been impacted by the Ti:Sapphire laser in some way. For the forseeable future, the Ti:Sapphire laser will continue to serve as the foundation of ultrafast technology and research.

References

[1] Berggren Wong and Schawlow. Far-infrared spectrum of $Al_2O_3:V^{4+}$. *The Journal of Chemical Physics*, 49(2):835–842, 1968.

[2] K.F. Wall and A. Sanchez. Titanium sapphire lasers. *The Lincoln Laboratory Journal*, 2(3):447 – 462, 1990.

[3] Anthony E. Siegman. *Lasers*. University Science Books, 1986.

[4] W. Koechner and M. Bass. *Solid-State Lasers: A Graduate Text*. Springer, 2003.

[5] Jianquan Yao and Yuyue Wang. *Nonlinear Optics and Solid-State Lasers*. Springer, 2012.

[6] Berggren Wong and Schawlow. Pulse evolution in a broad-bandwidth ti:sapphire laser. *Optics Letters*, 19(15):1149–1151, 1994.

[7] Kean Spence and Sibbett. 60-fsec pulse generation from a self-mode-locked ti:sapphire laser. *Optics Letters*, 16(1):42–44, 1991.

[8] Stark Albers and Huber. Continuous-wave laser operation and quantum efficiency of titanium-doped sapphire. *J. Opt. Soc. B.*, 3(1):134–139, 1986.

[9] Wall et al. Small signal gain measurements in a Ti:Al_2O_3 amplifier. *IEEE J. Quantum Electron.*, QE-24, 1988.

[10] Karl F. Renk. *Basics of Laser Physics*. Springer, 2012.

[11] Kogelnik et al. Astigmatically compensated cavities for cw dye lasers. *IEEE J. Quantum Electron.*, QE-8(3):373–379, 1972.

[12] M. B. Hooper. *Lasers Plasma Interactions 5: Inertial Confinement Fusion*. The Scottish Universities Summer School In Physics, 1995.

[13] Peter Moulton. Spectroscopic and laser characteristics of Ti:Al_2O_3. *J. Opt. Soc. B.*, 3(1):125–133, 1986.

[14] Steven T. Cundiff and Jun Ye. Colloquium: Femtosecond optical frequency combs. *Reviews of Modern Physics*, 75(1):197–246, 2003.

[15] John G. Eden. High-order harmonic generation and other intense optical field–matter interactions: review of recent experimental and theoretical advances. *Progress in Quantum Electronics*, 28(3):197–246, 2004.

[16] Genty Dudley and Coen. Supercontinuum generation in photonic crystal fiber. *Reviews of Modern Physics*, 78(4):1135–1184, 2006.

Appendix A: Pumping of a Degenerate 4-Level System

We have the relation between W_{14} and W_{41} in the presence of degeneracy:

$$W_{14} = \frac{g_4}{g_1} W_{41} \tag{25}$$

We write the rate equation for level 4:

$$\frac{dN_4}{dt} = W_{14}N_1 - W_{41}N_4 - \frac{N_4}{\tau_4} \tag{26}$$

which gives in steady state:

$$N_4 = \frac{W_{14}\tau_4}{W_{41}\tau_4 + 1} N_1 = \frac{W_{14}\tau_4}{\frac{g_1}{g_4}\tau_4 W_{14} + 1} N_1 \tag{27}$$

Using the conservation of atoms condition:

$$N = N_1 + N_2 + N_3 + N_4 \tag{28}$$

we plug in to find:

$$\begin{aligned} N_4 &= \frac{W_{14}\tau_4}{\left(1 + \frac{g_1}{g_4}\right) W_{14}\tau_4 + 1} (N - N_2 - N_3 - N_4) \\ \rightarrow N_4 &= \frac{W_{14}\tau_4}{\left(2 + \frac{g_1}{g_4}\right) W_{14}\tau_4 + 1} (N - N_2 - N_3) \end{aligned} \tag{29}$$

We also have the rate equation for levels 3 and 2:

$$\begin{aligned} \frac{dN_3}{dt} &= \gamma_{43}N_4 - \frac{N_3}{\tau_3} \\ &= \frac{W_{14}\tau_4\gamma_{43}}{\left(2 + \frac{g_1}{g_4}\right) W_{14}\tau_4 + 1} (N - N_2 - N_3) - \frac{N_3}{\tau_3} \end{aligned} \tag{30}$$

$$\begin{aligned} \frac{dN_2}{dt} &= \gamma_{42}N_4 + \gamma_{32}N_3 - \gamma_{21}N_2 \\ &= \frac{W_{14}\tau_4\gamma_{42}}{\left(2 + \frac{g_1}{g_4}\right) W_{14}\tau_4 + 1} (N - N_2 - N_3) + \gamma_{32}N_3 - \gamma_{21}N_2 \end{aligned} \tag{31}$$

Recalling the relation between N_2 and N_3 (independent of degeneracy):

$$N_2 = \left(\frac{\tau_{43}\tau_{21}}{\tau_{42}\tau_3} + \frac{\tau_{21}}{\tau_{32}}\right) N_3 = \beta N_3 \tag{32}$$

Combining the above 3 equations gives:

$$N_3 = \frac{W_{14}\tau_4\gamma_{43}}{\left(2 + \frac{g_1}{g_4}\right) W_{14}\frac{\tau_4}{\tau_3} + \frac{1}{\tau_3} + W_{14}\tau_4\gamma_{43}(1+\beta)} N \tag{33}$$

$$N_2 = \frac{W_{14}\tau_4\gamma_{43}}{\left(2 + \frac{g_1}{g_4}\right) W_{14}\frac{\tau_4}{\tau_3\beta} + \frac{1}{\tau_3\beta} + W_{14}\tau_4\gamma_{43}\left(1 + \frac{1}{\beta}\right)} N \tag{34}$$

The normalized population difference is:

$$\begin{aligned} \frac{\Delta N}{N} &= \frac{N_3 - \frac{g_3}{g_2}N_2}{N} \\ &= \frac{W_{14}\tau_4\gamma_{43}}{\left(2 + \frac{g_1}{g_4}\right) W_{14}\frac{\tau_4}{\tau_3} + \frac{1}{\tau_3} + W_{14}\tau_4\gamma_{43}(1+\beta)} - \frac{g_3}{g_2} \frac{W_{14}\tau_4\gamma_{43}}{\left(2 + \frac{g_1}{g_4}\right) W_{14}\frac{\tau_4}{\tau_3\beta} + \frac{1}{\tau_3\beta} + W_{14}\tau_4\gamma_{43}\left(1 + \frac{1}{\beta}\right)} \end{aligned} \tag{35}$$

Appendix B: Code for Matlab Plots

- Figure 5:

```
sigma = 3E-23;
tau43 = .1E-12;
tau3 = 3.2E-6;
spot = 200E-12;
hbar = 1.05E-34;
omega0 = 3.54E15;
P = linspace(0,7,1000);
deltaN = P./(P*((7*tau43/(2*tau3)) + 1) + (hbar*omega0*spot/(sigma*tau3)));
plot(P,deltaN,'LineWidth',3);

ylabel('Normalized Population Inversion');
xlabel('Pump Power (W)');
```

- Figure 7 & 8:

```
spot = 200E-12;

% PLOTS FOR PUMP POWERS 0W - 5W
Pin = linspace(0,5,10000);
Iin = Pin./spot;

% CIRCULATING POWER
Icirc = ((1.37E-9).*Iin - 1)*(1.29E9);
figure;
plot(Pin,subplus(Icirc)*spot,'LineWidth',3);
xlabel('Pump Power (W)');
ylabel('Circulating Power (W)');
% OUTPUT POWER
figure;
plot(Pin,subplus(Icirc)*spot*.07,'LineWidth',3);
xlabel('Pump Power (W)');
ylabel('Output Power (W)');

% PLOTS FOR PUMP POWERS 0W - 1W
Pin = linspace(0,1,10000);
Iin = Pin./(200E-12);

% CIRCULATING POWER
Icirc = ((1.37E-9).*Iin - 1)*(1.29E9);
Pin = Pin*1000;
figure;
plot(Pin,subplus(Icirc).*spot,'LineWidth',3);
xlabel('Pump Power (mW)');
ylabel('Circulating Power (W)');

% OUTPUT POWER
figure;
plot(Pin,subplus(Icirc).*spot*.07,'LineWidth',3);
xlabel('Pump Power (mW)');
ylabel('Output Power (W)');
```